Engineering Geology 264 (2020) 105321

Contents lists available at ScienceDirect

Engineering Geology

journal homepage: www.elsevier.com/locate/enggeo

# Stabilization by geomorphic reclamation of a rotational landslide in an abandoned mine next to the Alto Tajo Natural Park

Ignacio Zapico[a,*], Antonio Molina[b], Jonathan B. Laronne[d], Lázaro Sánchez Castillo[e], José F. Martín Duque[a,c]

[a] Geodynamics, Stratigraphy and Palaeontology Department, Complutense University, 28040 Madrid, Spain
[b] Centro de Astrobiología, CAB (INTA, CSIC), 28850 Torrejón de Ardoz, Madrid, Spain
[c] Geosciences Institute, IGEO (CSIC, UCM), 28040 Madrid, Spain
[d] Department of Geography and Environmental Development, Ben-Gurion University of the Negev, P.O. Box 653, Beer-Sheva 84105, Israel
[e] Department of Geologic Engineering, Polytechnic University of Madrid, Madrid 28003, Spain

ARTICLE INFO

*Keywords:*
Geomorphic reclamation
Landslide stabilization
Alto Tajo Natural Park
SfM-UAV
TLS
Geomorphic change detection

ABSTRACT

Two abandoned kaolin mines, surrounding one of the most outstanding natural parks of Spain, the Alto Tajo, have caused frequent environmental impacts. Within these are unstable areas prone to extensive mass movements that influence off-site sediment dynamics over the fluvial system. A waste dump in the Nuria mine obstructing a stream in the center of a valley experienced a rotational landslide. Mass movement between 2012 and 2014 was 0.025–0.026 m day$^{-1}$. To mitigate the high risk of an earthflow, a novel stabilizing surface drainage technique was implemented. Two remedial valleys designed with fluvial channels were constructed surrounding the landslide main body using natural landform design and regrading, with no need for artificial materials such as concrete or piles. This novel remediation process is generically termed geomorphic reclamation. The specific method applied to this site was GeoFluv with Natural Regrade software. Before (2014) and after geomorphic stabilization (2015–2017), the landslide was monitored using Digital Elevation Models (DEMs) of Difference (DODs) obtained by a Geomorphic Change Detection (GCD) tool. Two modern techniques, Terrestrial Laser Scanning (TLS), and, Structure from Motion photogrammetry combined with an Unmanned Aerial Vehicle (SfM-UAV), were used to acquire High-Resolution Topographies (HRTs) from which DEMs were derived. Data analysis and field monitoring results demonstrate that: i) the Nuria mine transformed almost 50% of the upper part of a natural catchment; ii) a waste dump active landslide with a surface rupture < 15m posed a high-risk hazard due to its continuous advance; iii) geomorphic reclamation succeeded in stabilizing the landslide during the monitoring period; iv) SfM-UAV-based topographies offer better accuracy and higher resolution, are cheaper and are obtained faster than TLS for mine areas.

## 1. Introduction

Landslides are widely studied natural phenomena (Highland and Bobrowsky, 2008) that can also be induced by anthropogenic activities such as mining (Carlà et al., 2018). Mines introduce new landforms to the landscape which can include tailing dams and terraced waste dumps with unstable slopes prone to erosion (Martín-Moreno et al., 2018), slope failures and landslides (Carlà et al., 2018). Several methods are used to avoid or mitigate landslide occurrence and impact. Site investigations usually rely on hazard evaluation techniques commonly using field inspection or aerial-photo interpretation, however, these techniques often provide insufficient detail to detect subtle landslides (Ortuño et al., 2017). More specific techniques, such as High Resolution Topographies (HRTs) obtained by Light Detection and Ranging (LiDAR) are useful for subtle events. LiDAR derived data, including slope, aspect or intensity (Mezaal and Pradhan, 2018) are combined with feature selection algorithms to detect and classify landslides. LiDAR techniques have been widely used in landslide analysis, because they allow obtaining HRTs based on point clouds with densities in the range 50–10,000 points m$^{-2}$ (Jaboyedoff et al., 2012). LiDAR is used in two procedures: Terrestrial Laser Scanning (TLS) and Aerial Laser Scanning (ALS). Which one is best used will depend on several considerations: size of area, range of vegetation, ground required target resolution and accuracy (Jaboyedoff et al., 2012).

An emerging technique to obtain HRTs is Structure from Motion (SfM) photogrammetry. It is widely used in different landscapes, such

* Corresponding author.
*E-mail address:* izapico@ucm.es (I. Zapico).

https://doi.org/10.1016/j.enggeo.2019.105321
Received 19 March 2019; Received in revised form 27 September 2019; Accepted 29 September 2019
Available online 24 October 2019

as rivers (Javernick et al., 2014), badlands (Carrivick et al., 2016) or natural landslides (Valkaniotis et al., 2018), yet is less common in mining areas (Xiang et al., 2018). Photographs can be obtained using different platforms, either hand-held using poles or masts, or Unmanned Aerial Vehicles (UAVs). The latter, usually known as drones, are the most commonly used method in the earth sciences combined with SfM (SfM-UAV) due to the ease of use, high flexibility and stability (Carrivick et al., 2016). They can be classified as: i) systems without their own propulsion: balloons, kites and paraglides; or ii) systems with engines: multirotors, fixed wings, airship and helicopters (Nex and Remondino, 2014). A multirotor is the best suitable UAV for surveying steep-slope small landslides since it allows the operator to take oblique photographs close to the landslide, thereby increasing image resolution (Giordan et al., 2015).

HRTs are not only capable to detect landslide events, but also to monitor them (Giordan et al., 2013). For instance, by using SfM, Lucieer et al. (2014) calculated a 0.01-0.038 m $day^{-1}$ landslide velocity displacement. Analyses of HRTs and Geomorphic Change Detections (GCD) tools define erosion/deposition zones, volumetric data and sediment budgets (Baldo et al., 2009). The most widely used methodology and software is Geomorphic Change Detection (GCD, 2015). Although it has been widely used in natural landscapes, few examples have been published on mining areas (Xiang et al., 2018; Zapico et al., 2018).

Once a landslide has occurred, a variety of earth slope stabilization/mitigation techniques can be carried out: excavation, backfilling with lightweight material, benches, check dams, retention walls, biotechnical approaches and piles (Highland and Bobrowsky, 2008). These techniques are usually expensive, and their success is limited to small landslides. Walls and piles are commonly used, yet tend to fail due to an inability to manage a large amount of unstable soil, or, by being anchored to the landslide instead of to the deep slip surface (Di Maio et al., 2018).

It is widely accepted that the key issue to mitigate/stabilize a landslide arises in proper management of surface and subsurface water (Highland and Bobrowsky, 2008; Yu et al., 2019). Surface drainage techniques, constructed with rigid elements such as concrete or pipes, are more effective than retaining walls and piles, as they prevent erosion of the face, reduce surface slumping and most importantly avoid water infiltration. Further, they require minimal design and installation cost.

An inventive approach of surficial drainage management, more adaptive and 'ecological', is Fluvial Geomorphic Reclamation (Bugosh and Epp, 2019). It is an emerging technique for the rehabilitation of land disturbed by earth movements, to achieve long-term erosion stability. However, geomorphic reclamation has not been used before now to stabilize mass movements.

The most important kaolin mining activity in Spain is located close to the Alto Tajo Natural Park. Here, abandoned mines increase sediment yield of the fluvial network due to their unstable landforms and lack of erosive-sedimentary control measures (Zapico et al., 2017, 2018). Some of these mines contain massive landslides, the largest occurring in the abandoned Nuria mine in the Matalacascabras stream catchment. This was a rotational landslide (slump) with a continuous advance. In 2014–2015 an innovative solution was carried out to stabilize the landslide with a surface drainage based on geomorphic reclamation. Both, the landslide ground as well as the geomorphic stabilization region, have been topographically monitored principally using TLS, and by SfM-UAV. The aims of this study are: i) to quantify global earth movements due to mining activity in the Matalascabras stream catchment; ii) to characterize the shape and displacement of the Nuria landslide; iii) to describe a geomorphic stabilization technique based on replicating two 'natural' channels and small valleys; iv) to monitor landslide stability; and v) to evaluate the SfM-UAV technique as an alternative to TLS in complex topographies such as mining areas.

## 2. Materials and methods

### 2.1. Study area

The highest amount and best-quality kaolin product in Spain is extracted at several mines surrounding the Alto Tajo National Park (Fig. 1). This kaolin is the Arenas de Utrilllas Formation clay matrix of silica sands of fluvial origin deposited underneath marine carbonate limestone and dolostone. This cake-like terrain of silica sands (below) and limestone and dolostones (above) were deposited in the Iberian Mesozoic sedimentary basin during the Upper Cretaceous. The sediments were later uplifted as a plateau and slightly folded and faulted in an Alpine orogeny to form the Iberian Mountain Range. The incision of the Tajo River and its tributaries into this plateau left characteristic landforms of mesas, cuestas and perched synclines, standing above a dense network of fluvial canyons with steep and long slopes. This is where the kaolin mines, including the Nuria mine, are located.

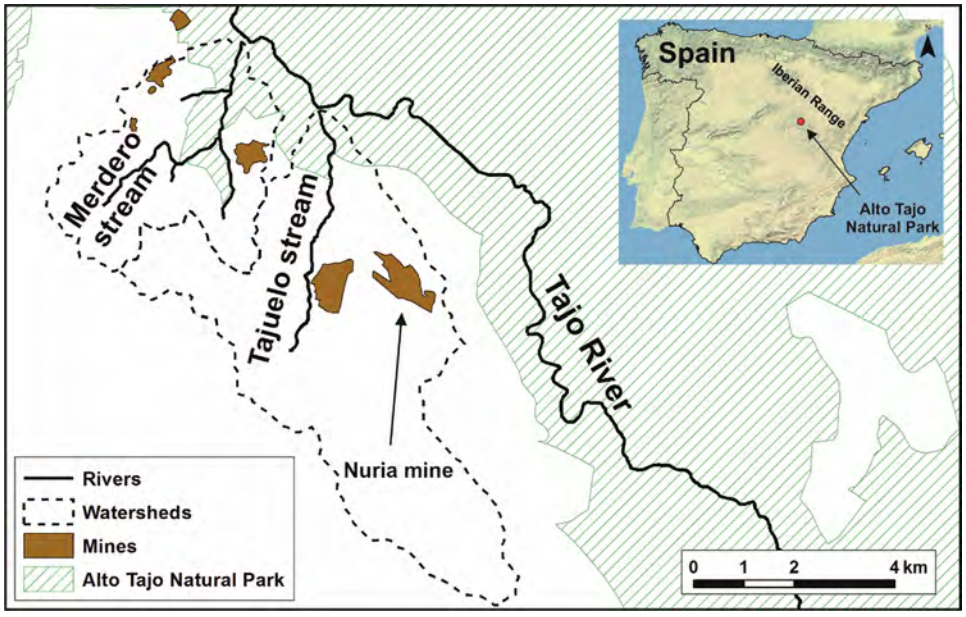


**Fig. 1.** Location of the Alto Tajo Natural Park and the Nuria mine. Redrawn from Zapico et al. (2018).

The slopes are draped by characteristic carbonate colluvia, the substrata of calcaric cambisols which support dense and ecologically valuable *Pinus nigra* subsp. *salzmannii* and *Quercus faginea* forests. This physiographic setting is influenced by a temperate and continental Mediterranean climate, with a mean annual precipitation of 783 mm, and a mean annual temperature of 10 °C. Additional information on the geological and environmental setting is included elsewhere (Zapico et al., 2017, 2018).

The Nuria mine, formerly operated by the CAOSIL company, is one of the two abandoned mines in the Alto Tajo. Located in the Tajuelo stream watershed (Fig. 1), it operated during 1982–2011 by the contour mining method in the upper sub-watershed termed Matalascabras. Between the end of the mining activity and this stabilization intervention, the large landforms of the mine include (Fig. 2-D): i) a large open pit 1.67 km in length and a highwall on average 70 m in height; ii) two large ponds in the open pit base; iii) a waste dump restored by gradient terraces located on the true left valley; and iv) a waste dump restored by gradient terraces in the center of the valley, obstructing drainage in the ephemeral channel.

Fig. 2 shows the temporal change of this minescape: A) before mining activity ensued, the topography of the Matalascabras watershed was typical of a stable mountain catchment (1970s); B) at an initial stage, the contour mine configuration was an open pit with a waste dump made in gradient terraces (1985–2002) with 7 m high outslopes and a 50% gradient slope; C) accumulated mine debris filled the stream valley (2002–2006) with a final configuration of two overstepped, 53 m terraced slopes with a 50% gradient; and D) terraces affected by erosion and landslides were repaired and rebuilt several times between 2006 and 2011 to retain the terraced configuration. Finally, the terraces experienced a large rotational landslide (Fig. 3) with a toe advancing several centimeters per week, evolving into an earthflow (2012–2014). The onset date of this landslide has not been documented. However, the initial landslide occurred after 13.07.2012, the date of an aerial photo of the Spanish National Geographic Institute (PNOA, 2012). Hence, the July 2012 date is adopted for this study as the threshold date for the landslide.

The Nuria mass movement is a typical rotational landslide. Specifically, it is a debris (mine waste) slump (Fig. 3). The exposed cracks are concentric in plan and concave toward the direction of movement. This combination of features results in a typical spoon-shaped landform, perfectly depicted in Figs. 3-B and C that show the most characteristic slump elements.

Since the geometry of the shear surface is not known and these are rarely a spherical segment of uniform curvature, or that there may be several rupture surfaces, we applied a rough interpretation of the thrust to be a classic, purely rotational slump. The concept was to utilize a circular arc between the main scarp of the slide head (crown) and the location where the surface of rupture intersects the original slope (pre-landslide). These two arc locations were clearly identified by comparing the pre-and post-landslide topographies (Fig. 3A). The rotated mass occupies the upper half of the original slope, therefore the maximum depth of the rupture surface at the center of the main body of the landslide is *circa* 15 m. Other dimensions of the landslide are a total length of 160 m, a maximum width of 140 m, widths of 90 m at the head and 50 at the foot, and 45 m of difference in height between the crown and the toe tip. Fig. 3D illustrates the spatial position of the remedial activities undertaken within the topography of the rotational landslide.

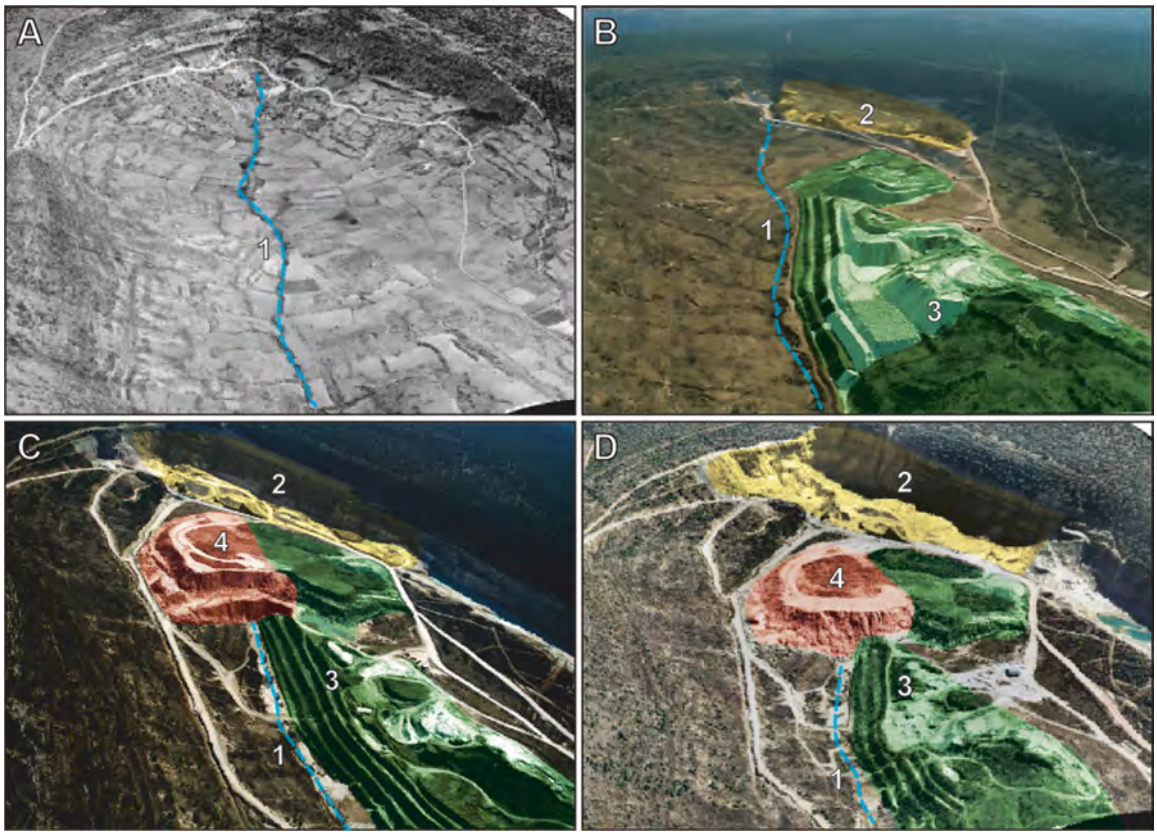


**Fig. 2.** The temporal evolution of the upper Matalascabras catchment and Nuria mine configuration. (A) 1970s topographic 3D view (source Fototeca IGN); (B) Aerial oblique photo (*circa* 1989–1992, by Paisajes Españoles); (C) 2002 oblique photo (source Paisajes Españoles); (D) 2009 topographic 3D view (PNOA, 2009). The 3D views were generated with ArcGIS Pro software by combining the two orthophotos with their respective Digital Elevation Models (DEM).1: the Matalascabras ephemeral stream; 2: open pit with a highwall and two ponds; 3: terraced and reclaimed waste dumps; 4: terraced waste dam blocking the Matalascabras stream where the Nuria rotational landslide occurred.

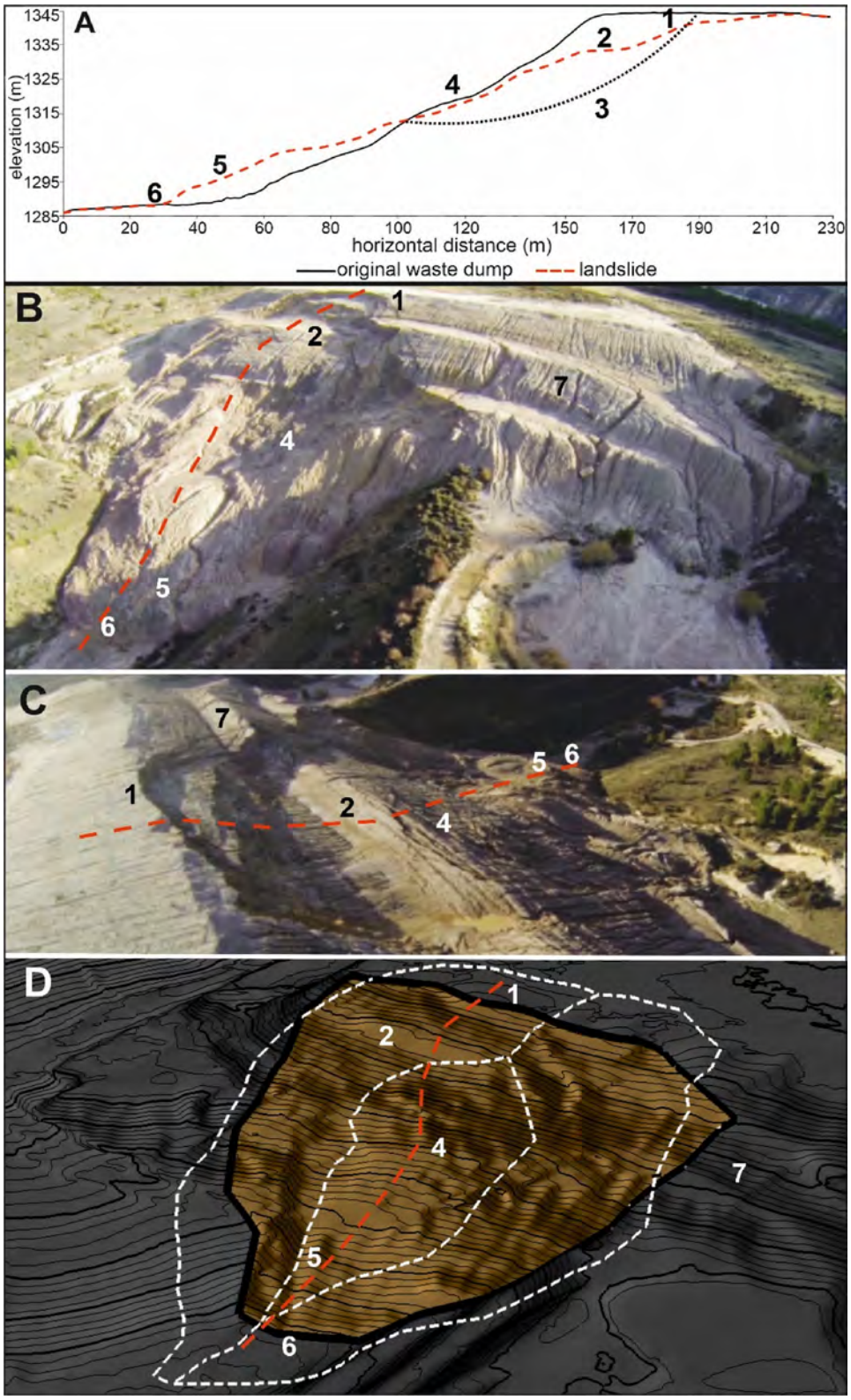


**Fig. 3.** Nuria landslide characterization: longitudinal profile before and after the landslide (A); oblique photographs (B, C) and 3D topographic view (D) of the Nuria landslide before the geomorphic stabilization. (1) crown and main scarp; (2) head; (3) surface of rupture; (4) main body; (5) foot; (6) toe; (7) original terraced waste dump with severe rill and gully erosion. The dotted polygons at (D) divides the landslide in three sectors — the unreclaimed landslide main body, and two lateral valleys, to be designed and built with geomorphic reclamation, which join at the landslide toe, where a rockfill was also planned to be built (6). Photos by DGDRONE (2014).

### 2.2. Geomorphic stabilization

A geomorphic approach to stabilize the Nuria landslide was planned during 2014 with earth movement regrading commencing in December of the year. This solution combined three universal stabilization measures, based on a landform regrading of the unstable mass: i) removing weight from the upper part of the landslide; ii) draining the entire mass in terms of runoff and groundwater; and, iii) reinforcing the resistance of the toe by accumulating mass at this position. These measures avoid the use of artificial materials such as concrete or piles. Specifically, the steps were as follows:

1 A rockfill was placed at the slump toe to act as a natural buttress (Fig. 3D). These rocks were available within the mine.

2 Earth was removed near the slump scars and spread in two large, horseshoe-shaped earth lobes. Thus, pressures due to overburden were released.
3 Two valleys (Fig. 3D) with channels were `sculpted' into the earth lobes, to steadily drain both runoff and groundwater. Specifically, each valley bottom acted as an "aquifer window" to decrease groundwater levels, thereby reducing the likely origin of the slumping.

The novelty in this approach is that stabilization was carried out following a geomorphic reclamation approach using the GeoFluv method (Bugosh, 2000).

GeoFluv is a fluvial geomorphic method for land reclamation that helps the user to design landforms that naturally would form by erosional processes under the climatic and physiographic conditions at the site. A suitable and stable reference area is identified to provide critical input values for the reclamation design. Natural Regrade is the software that allows users to rapidly make and evaluate GeoFluv designs in a CAD format from the input values. Zapico et al. (2018) and Bugosh and Epp (2019) describe in detail the method and its successful use in mine reclamation projects. To the best of the authors' knowledge, this is the first instance where the GeoFluv method has been used to design a combined drainage and pressure release solution to stabilize a mass movement phenomenon.

### 2.3. Topographic monitoring and data analysis

Topographic monitoring was divided into three periods: i) 1984–2012, to characterize and quantify the earth movement due to mining in the Matalascabras catchment; ii) 2012–2014, to study the waste dump landslide; and iii) 2015–2017, to monitor the extent of stabilization of the geomorphic design.

#### 2.3.1. Topographic sources and surveys

Various topographic sources (Table 1) have been used for the study: i) a 1:25,000 topographic map with 1 m equidistant contour (IGN, 1995); ii) public high resolution LiDAR data surveyed by ALS and provided by the Spanish National Plan for Aerial Orthophotography (PNOA, 2009); iii) four scanned topographies obtained by TLS (before the geomorphic stabilization by regrading was initiated, December 2014; at the end of construction activity to stabilize the landslide, August 2015; post-landslide geomorphic stabilization, July 2016 and November 2017); and, iv) a topography surveyed by SfM-UAV in November 2017.

TLS-based HRTs were produced with a Leica MS60 multi-Station (MS60) (Table 1) and processed with the LP360 Advanced edition software (Qcoherent software LLC, 2015) following the same procedure used in other topographic monitoring activities in the area (Zapico et al., 2018). Each TLS survey was performed from multiple positions along the landslide and its vicinity to reduce a shadow effect in the final point clouds (Table 1). Two topographies (2016 and 2017) were surveyed with several check points; the root-mean-square error (RMSE) was used to determine the accuracy of height (RMSEZ) following the guidelines of the American Society for Photogrammetry and Remote Sensing (ASPRS, 2014). All scans were undertaken using the same field procedure, hence, the average RMSEZ was used for the following TLS topographies (Table 1). The 1:25,000 topographic map dated 1984 does not have an accuracy value. As in other studies, it was derived based on a direct comparison with the 2009 topographic data of those areas without topographic changes between the two dates (Giordan et al., 2013).

During the final TLS survey, an UAV paired with SfM image processing (SfM-UAV) survey was conducted to evaluate its potential future use to monitor this geomorphic stabilization and the evolution of other mining landforms in the area. Altogether, 708 80% overlapping photographs were collected with programmed flights from both zenithal (512) and oblique angles (196) by a DJI Phantom 4 Pro drone. Both sets were obtained keeping the drone at a constant altitude, with a 65.7 m maximum height above the ground to ensure a desirable minimum Ground Sampling Distance (GSD) of 1.81 cm $pix^{-1}$. Nineteen fixed targets were placed along the area as check (7) or control (12) points. Their coordinates were measured with the MS60. Photographs taken from different angles and control points reduce possible systematic DEM deformations common in SfM-derived topographies (James and Robson, 2014; Carrivick et al., 2016). Photos and control points were processed with Agisoft PhotoScan (Agisoft LLC, 2016). One of the most time-consuming steps with Agisoft is the generation of dense point clouds, and it widely varies depending on the chosen quality setting. The accuracy of the final topography and the point density was analysed depending on medium, high and highest options, as well as depending on whether oblique photos were added to processing.

#### 2.3.2. Landslide displacement analysis

The 2009 and 2014 topographies were used to elaborate hillshaded DEMs and contours to estimate toe displacement. This was also directly measured in the field by use of 40 cm wooden sticks as reference. One set of sticks was fixed in the landslide toe. Another set was fixed in a natural, stable surface located downslope from the landslide to determine the temporal variation of distances between both sets. The first

**Table 1**
Topographic data availability and related accuracy.

| date | source/method | n° photos or scan positions | point cloud density | RMSE check points | | |
|---|---|---|---|---|---|---|
| | | | | n° of check points | x,y | z |
| | | # | pts $m^{-2}$ | # | m | |
| 1984[1] | 25,000 topographic map with 1 m equidistant contour | n.d. | n.d. | n.d. | n.d. | 1.93[3] |
| 2009[2] | LiDAR-ALS | n.d. | 0.35 | n.d.[4] | 0.3[4] | 0.2[4] |
| 04.12.2014 | LiDAR-TLS | 5 | 17.45 | n.d. | 0.079[5] | 0.04[5] |
| 25.08.2015 | LiDAR-TLS | 8 | 109.58 | n.d. | 0.079[5] | 0.04[5] |
| 13.07.2016 | LiDAR-TLS | 12 | 101.79 | 9 | 0.089 | 0.041 |
| 01.11.2017 | LiDAR-TLS | 12 | 122.69 | 13 | 0.068 | 0.038 |
| 01.11.2017 | SfM-UAV | 708 | 1,061.84 | 7 | 0.009 | 0.009 |

n.d. - no data.
[1] This map was published in 1995, however, it was prepared with photogrammetric data dated 1984.
[2] This is the most recent topography data prior to the 13.07.2012 landslide, to represent the pre-landslide topographic conditions.
[3] Derived from a direct comparison with 2009 topographic data of those areas without topographic changes between the two dates.
[4] Technical specification (PNOA, 2009).
[5] Average value based on 2016 and 2017 accuracies.

measurement was conducted on 07.11.2014 and the second on 03.12.2014, immediately prior to geomorphic stabilization. The monitoring term was 27 days.

#### 2.3.3. Volume budget through DEM comparison

A DEM was derived from each topography (Table 1) and DEMs of Difference (DoDs) were obtained by using the GCD software (GCD, 2015), similar to other analyses undertaken in the Alto Tajo area (Zapico et al., 2018). A specific DEM cell size was defined for each DoD comparison, based on the lowest resolution to account for the different topological resolutions (Table 1). This is an important factor, because volume data can vary depending on DEM grid size for a given raw topography.

DoD comparisons yielded terrain volumes that were transformed to mass of sediment by using 1.2. g $cm^{-3}$ as bulk sediment density (Zapico et al., 2018). The comparisons also supplied an image showing those areas. DoDs were used to quantify four different masses:

1 the mass of global earth movement (removed/accumulated) in the Matalascabras valley due to mining activity for the period;
2 the mass of depleted/accumulated sediment owing to the rotational landslide;
3 the mass of earth movement (removed/accumulated) during the geomorphic stabilization; and
4 erosion/deposition of sediment and the annual sediment yield due to the geomorphic stabilization surrounding the regraded and ungraded landslide main body.

## 3. Results

### 3.1. Mining earth movement in the Matalascabras valley. Landslide footprint and displacement

The earth movement analysis shows : 7,766,000 $m^3$ +/− 15 % of sedimentary rocks were removed by mining in highwalls and pits; and, 11,569,000 $m^3$ +/− 14% of mine spoils were deposited in waste dumps in the Matalascabras Valley (Tables 2a and b). The Nuria rotational landslide topographical change investigation, illustrated at Fig. 4A, shows: i) a main scarp has appeared in the upper part (red areas) due to landslide depletion (60,500 $m^3$ +/− 5 %) and ii) waste material has been displaced and accumulated (27,300 $m^3$ +/− 7 %) in the lowest part (blue areas), shaping the landslide's toe.

By comparing the positions of the landslide toe in 2014 with the inferred original waste dump situation in 2012 (Fig. 5) the calculated landslide advance is 20.7 m in 28 months, averaging 0.025 m $day^{-1}$. From the 2014 field measurements by wooden sticks, the landslide's toe displacement was 0.7 cm in 27 days (on average 0.026 m $day^{-1}$).

### 3.2. Geomorphic stabilization design and construction

The geomorphic design of two small valleys located on the sides of the landslide main body to stabilize the Nuria landslide is shown in Fig. 6. Each drainage area includes a steep "Aa + channel" (Rosgen, 1994) with a zig-zag pattern, rounded interfluves and swales. The average gradient of the constructed channels is 20 percent. The ridges and swales have average slopes of 20 and 25 percent, respectively.

Fig. 4B displays a DoD showing the earth movement involved in the construction of the geomorphic stabilization: 28,000 $m^3$ +/− 2 % were removed and 25,000 $m^3$ +/− 2 % were accumulated. Fig. 7B shows a detailed view of the landforms shaped during the construction. Subridges split run-off towards the small swale su B-C atchments, reducing erosive energy through concavity, conveying runoff toward the zig-zag main channel (Fig. 7B). These channels also have concave longitudinal profiles, instead of the original terraced profile (Fig. 7D), reducing shear stress and stream power. The two channels that form the main elements of the geomorphic stabilization (Fig. 7C) were constructed, removing up to 8 m of earth from the upper parts of the landslide and filling as much as 4 m in the lower areas (Fig. 7D). The entire earth movement was completed by using an excavator and a bulldozer. The central part of the main body of the landslide could not

**Table 2**
Temporal topographic changes in the Nuria mine area.

A

| change | date | | area | | topographic changes | | |
|---|---|---|---|---|---|---|---|
| | initial | final | zone | surface | area with detectable changes | erosion/ removal*/ depletion** | error (+/-) |
| | | | | ha | % | $m^3$ | % |
| 1 | 1984 | 2009 | upper Matalascabras valley | 287 | 49.6 | 7,766,000* | 15 |
| 2 | 2012[1] | 2014 | full landslide | 2.9 | 81.4 | 60,500** | 5 |
| 3 | 2014 | 2015 | geomorphically stabilized landslide | 2.2 | 96.3 | 28,000* | 2 |
| 4 | 2015 | 2016 | unreclaimed landslide main body | 0.7 | 33.2 | 686 | 16 |
| 5 | | | geomorphically stabilized landslide | 2.2 | 13.6 | 549 | 22 |
| 6 | 2016 | 2017 | unreclaimed landslide main body | 0.7 | 19.2 | 234 | 4 |
| 7 | | | geomorphic stabilized landslide | 2.2 | 10.0 | 297 | 27 |

B

| change | topographic changes | | | | | |
|---|---|---|---|---|---|---|
| | deposition/ accumulation*** $m^3$ | error (+/-) % | total sediment yield Mg $ha^{-1}$ | error (+/-) % | annual sediment yield Mg $ha^{-1}$ $yr^{-1}$ | error (+/-) % |
| 1 | 11,569,000*** | 14 | n.d. | n.d. | n.d. | n.d. |
| 2 | 27,300*** | 7 | n.d. | n.d. | n.d. | n.d. |
| 3 | 25,000 | 2 | n.d. | n.d. | n.d. | n.d. |
| 4 | 248 | 14 | 751 | 27 | 819 | 27 |
| 5 | 184 | 27 | 199 | 36 | 217 | 36 |
| 6 | 97 | 27 | 235 | 46 | 188 | 46 |
| 7 | 158 | 28 | 76 | 66 | 60 | 66 |

n.d. - no data.
[1]Although this topography was surveyed in 2009, it is reasonable that it represents the waste dump configuration at the onset of the landslide.

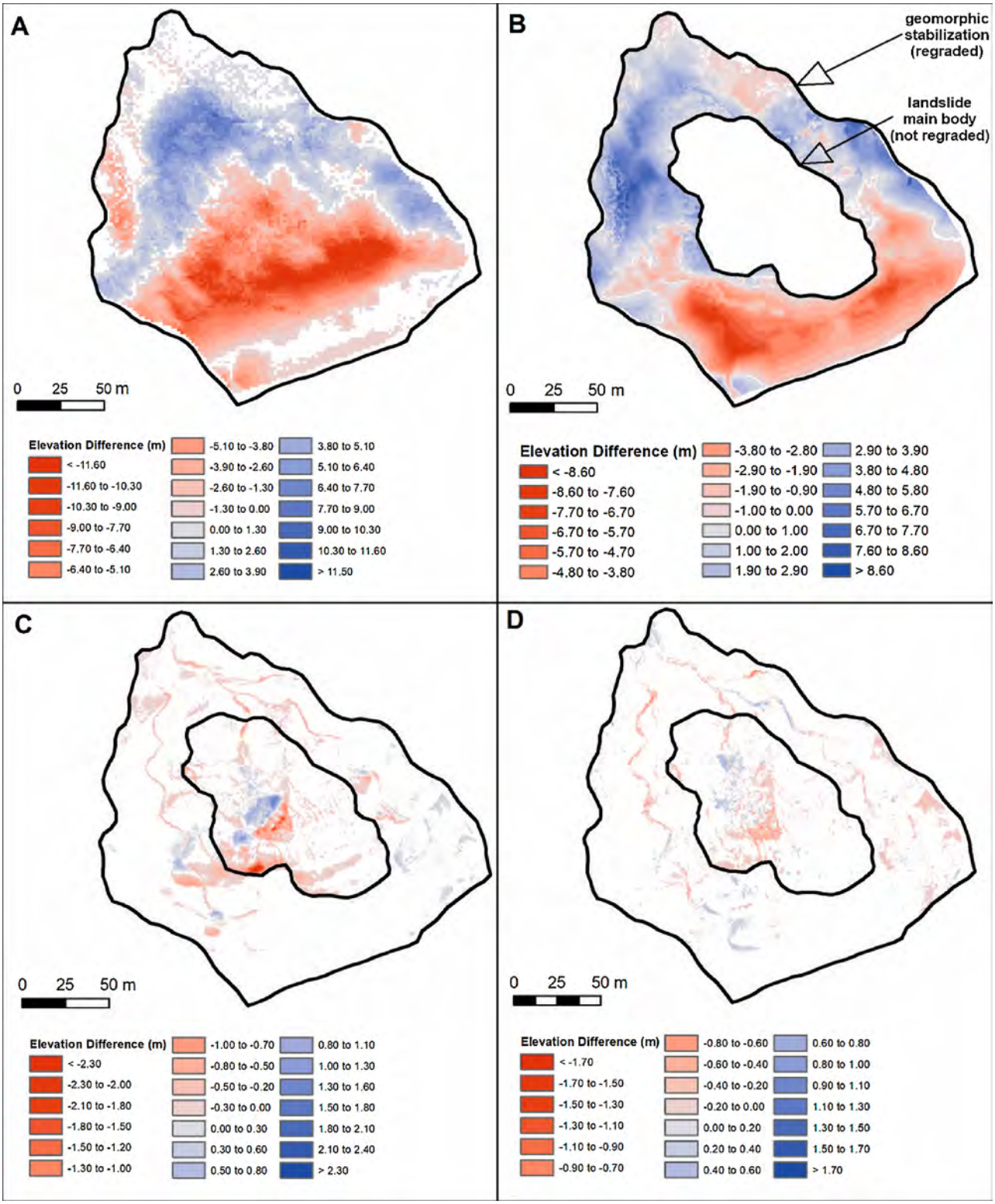


**Fig. 4.** DoDs for the Nuria landslide for different periods of time. (A) 2012–2014, landslide occurrence; (B) 2014–2015, geomorphic stabilization by earth regrading activities; (C) 2015–2016, after the first year of geomorphic stabilization (D) 2016–2017, after the second year of geomorphic stabilization.

be regraded within this project, due to groundwater saturation at the time of construction and budget constraints, yet, it will be reshaped in the near future using the same approach.

The geomorphic stabilization was finalized by spreading an onsite carbonate colluvium topsoil cover over the regrading (Fig. 7A) and seeded with suitable species (Zapico et al., 2018). Fig. 8A shows an oblique aerial view of the final geomorphic stabilization.

The stabilization procedure followed a 'fluvial geomorphic approach', creating a steady-state landscape by 'sculpturing' two mature valleys in the unstable landslide mass (Toy and Chuse, 2005). The process of excavating these two valleys combined geotechnical and hydrological stability. The geotechnical stability was obtained by

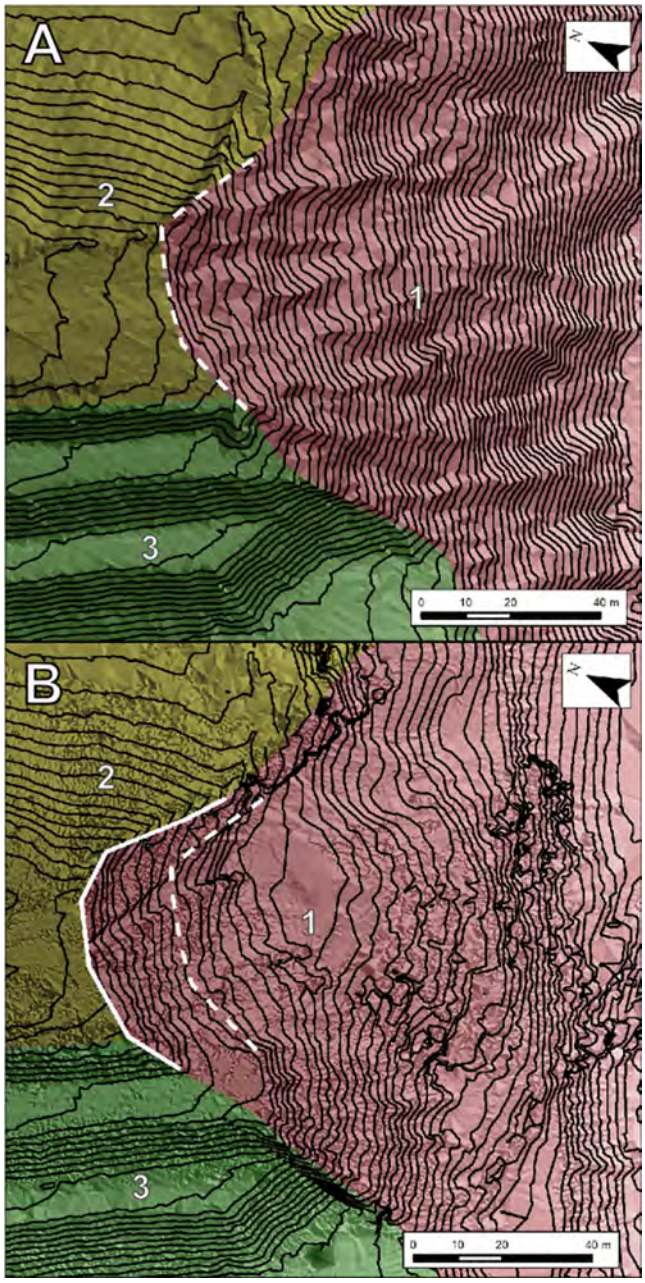


**Fig. 5.** 2D views of the Nuria waste dump (1) toe before (A, 2012) and after (B, 2014) the landslide. The dotted line represents the inferred position of the 2012 terraced waste dump tip; the continuous line shows the position of the 2014 landslide toe. (2) the Matalascabras Valley; (3) terraced-restored waste dump.

removing mass from the upper part of the landslide and accumulating it at the toe, as well as by draining the entire mass of runoff and groundwater. The hydrological stability was achieved by introducing core principles of the GeoFluv-Natural Regrade method: splitting the runoff in 0-order watersheds (swales), adding concavity to the entire set of hillslopes facing the channels, and by the meandering (zig-zag) pattern of the channels, which, in turn, also have concave longitudinal channel profiles. The combination of these topographic factors slowed water velocity, thereby reducing erosion.

### 3.3. Monitoring the geomorphic reclamation

Figs. 4C and D show the DoDs for the two monitoring years after the geomorphic stabilization: 2015–2016 and 2016–2017. The sediment yield of the unreclaimed landslide main body, representative of the pre-stabilization scenario, was very high, especially during the first monitoring year (819 Mg $ha^{-1}$ $yr^{-1}$ +/− 27 %). After the second year it decreased to 188 Mg $ha^{-1}$ $yr^{-1}$ +/− 46%. Sediment yield in the geomorphically regraded (stabilized) zone, although high during both periods, was 217 +/− 36 % and 60 +/− 66 % Mg $ha^{-1}$ $yr^{-1}$, respectively (Tables 2a and b). For these regraded areas, most of the erosion occurred in the channels (Figs. 4C, D), covering 10–13.6 % of the area.

In terms of landslide stability, none of the two regraded areas experienced significant mass movement displacements (Figs. 4C, D) unlike the situation prior to 2014 (Figs. 4A and 5). Both the geomorphically stabilized/regraded area and the unreclaimed landslide main body experienced two very small shallow landslides during the first monitoring year (Fig. 4C). They remained stable thereafter (Fig. 4D and 8 B and C).

### 3.4. Comparison of SfM-UAV and TLS

A general overview of the SfM-UAV topography surveyed in 2017 and processed with Agisoft using “high quality” dense cloud setting is shown in Fig. 9A. This topography has a vertical accuracy of 0.009 m, and 0.019 m when merely planar photos are used. In both cases, dense cloud quality settings do not widely vary data accuracy (Table 3). In comparison with the TLS results, the SfM-UAV topographies have better accuracy and point cloud density. Moreover, the TLS produced several shadows within channels and rills (Figs. 9B, C).

There are large differences between TLS and SfM-UAV with respect to production of topography. TLS required 16 h in the field, whereas SfM-UAV required 2.8–3 field hours. However, TLS topography required no post-processing time to produce a raw point cloud, whereas for SfM-UAV this time span varied between 3.5 and 58.5 h, depending on the photos and settings used. The longer post-processing times for SfM-UAV are primarily required for a computer rather than by personnel.

## 4. Discussion

The mining activity of the Nuria site altered almost 50% of the upper part of the Matalascabras catchment, a tributary of the Tajo River. Specifically, 7.8 million $m^3$ +/− 15 % of sedimentary rocks were removed (‘eroded’) by mining in highwalls and pits, and 11.5 million $m^3$ +/− 14 % of mine spoils were deposited in the catchment as waste dumps during 25 years (see Fig. 2). The excess of waste dump volume compared to the mined volume is due to the swelling factor of the overburden and to the fact that residues of kaolin processing were also deposited within the mine. One of the waste dumps blocked the Matalascabras valley and experienced a large rotational landslide in 2012, requiring stabilization to avoid an earthflow.

Before the geomorphic stabilization was undertaken, the landslide advanced 0.025–0.026 m $day^{-1}$. This is similar to other landslide velocities reported in the literature, such as the Home Hill landslide in Tasmania, advancing 0.01–0.038 m $day^{-1}$ (Lucieer et al., 2014) or the Latronico landslide in Italy, monitored to move 0.01–0.07 m $day^{-1}$ (Di Maio et al., 2018). In addition, the Nuria landslide had an earth displacement of 60,500 $m^3$ +/−5 %, similar in magnitude to other landslides such as the Okeanos landslide in Greece, moving 93,000 $m^3$ (Valkaniotis et al., 2018).

### 4.1. Geomorphic stabilization of the Nuria landslide

Among all landslide stabilization/mitigation techniques, in most cases drainage methods are the most effective, because they can adequately drain surface and ground water (Highland and Bobrowsky, 2008; Yu et al., 2019). The Nuria landslide was stabilized by ‘sculpting’ two ‘natural’ small valleys with non-structural fluvial channels,

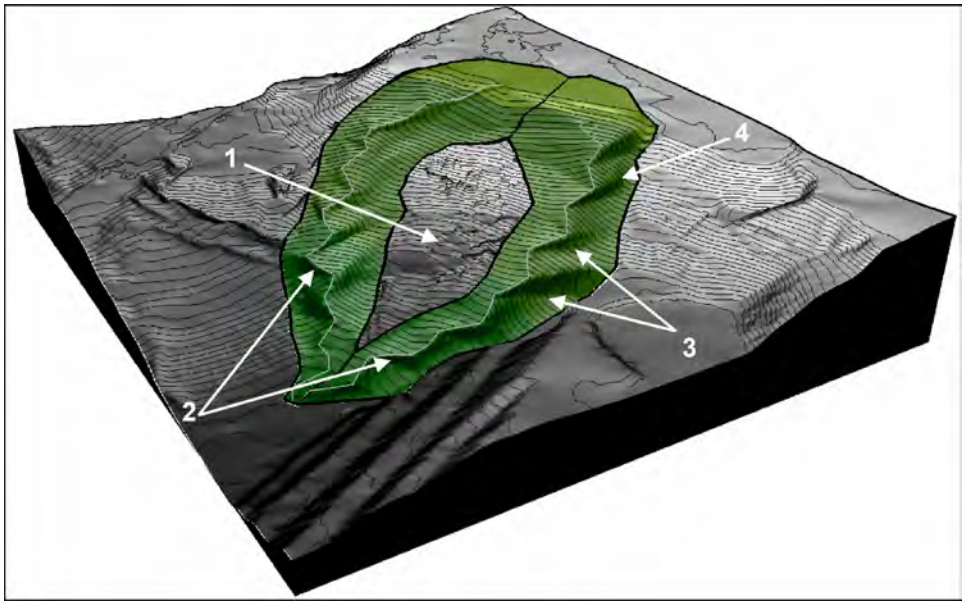


**Fig. 6.** A 3D view of the geomorphic design for the Nuria landslide stabilization. (1) unreclaimed landslide main body; (2) main channels; (3) convex-concave subridges; (4) predominantly concave swales.

designed with geomorphic reclamation techniques, instead of using engineered channels or underground drains (Highland and Bobrowsky, 2008). The geomorphic stabilization involved 28,000 $m^3$ +/− 2 % of earth cut and 25,000 $m^3$ +/− 2 % of earth filled, the difference due to compaction of fill.

After the stabilization was completed no mass movement displacement was recorded (Figs. 4C, D and 10 ), outside two very small shallow landslides, interpreted as re-adjustments. The ongoing success of this stabilization was achieved by using a geomorphic reclamation technique of design and construction, specifically GeoFluv-Natural Regrade (Figs. 6 and 7). The two lateral channels are capable to drain surface and ground water from the unreclaimed landslide main body. The maximum depth of the surface of rupture was 15 m, and the built channels cut 7 to 9 m at the head, to intersect the surface of rupture or end close to it. This, in addition of removing mass, decreased infiltration and increased aquifer draining, preventing the effect of groundwater pore pressure. The success of this approach led local authorities to extend this solution to nearby areas, thereby improving the entire drainage pattern (see Fig. 8B and C), and will soon be applied to the unrestored landslide main body area.

This approach is similar to another novel landslide mitigation drainage technique based on siphons and inclined boreholes (Yu et al., 2019). Its benefits contrast with other attempts to stabilize landslides with walls or piles that have failed (Di Maio et al., 2018). Admittedly, piles have successful results in some cases (Şengör et al., 2013), but they are expensive and require maintenance.

Although the main aim of this study and of the applied solution was the geomorphic stabilization of the mass movement, additional points of discussion can be raised regarding erosion monitoring. The initial values of the unreclaimed main body area during the first monitoring year (819 Mg $ha^{-1}$ $yr^{-1}$ +/−27) are very high, more than double the sediment yield in equivalent nearby areas such as the Santa Engracia mine - 353 Mg $ha^{-1}$ $yr^{-1}$ (Martín-Moreno et al., 2018). This value represents the extremely high geomorphic instability before this corrective intervention. After geomorphic stabilization, the erosion of the unreclaimed landslide main body was still high, 188 Mg $ha^{-1}$ $year^{-1}$ +/− 46%, but with a 77 % reduction, related, for example, to solving the run-on effect due to the geomorphic solution.

The new valleys of the geomorphically stabilized areas have produced high sediment yields during the first monitoring year (217 Mg $ha^{-1}$ $year^{-1}$ +/− 36 %) although this figure was drastically reduced to 60 +/− 66 % Mg $ha^{-1}$ $year^{-1}$ during the second year. These latter values can be considered more than acceptable, considering both the reported values for mine rehabilitated areas and the challenging circumstances of this geomorphic reclamation, with 20% gradient slopes of longitudinal profile channels 'sculpted' on un-consolidated materials. Although monitoring has not been conducted after 2017, aerial views from 2019 (Fig. 8C) and onsite ground inspections show very high stability of the channels. While recognizing the short-term stabilization success, the Nuria landslide requires ongoing monitoring to evaluate the long-term extent of geomorphic stabilization.

### 4.2. Topographic methods

The DoD grid comparison allowed quantifying earth movement in terms of erosion/removal and deposition/accumulation, thereby quantifying long and short-term mining impacts and the effect of geomorphic stabilization. This has been made possible due to accuracy and cell size, having been measured and adapted for each topography and for each comparison. Accuracy was measured twice for the topographies surveyed in the field with TLS. However, all the scans were surveyed with the same instrument and following the same field procedure, hence we assume 2016–2017 average sample accuracy is representative of all scans. TLS accuracy varied among 3.8 and 4.1 cm similar to other studies, where it was determined to be ≤ 5 cm (Carrivick et al., 2016; Victoriano et al., 2018; Zapico et al., 2018). This study confirms previously demonstrated outcomes for landslide and debris flow in steep natural watershed areas (Victoriano et al., 2018), that both LiDAR data and DoD comparisons are suitable tools to monitor landslides in mining areas.

The 12 control points to georeference the SfM-UAV topography are in the range of values suggested by others. For instance, Agüera-Vega et al. (2017) suggested 15 whereas Tonkin and Midgley (2016) recommended four. The SfM-UAV topography produced higher vertical accuracy than the TLS-based topography in the range 0.9–1.9 cm depending on the use of oblique photos. These values are similar to findings from others in landslide and gully literature: 2.5–4 cm (Harwin and Lucieer, 2012) or 1.4–6 cm (Lucieer et al., 2014). The present study also highlights the importance of oblique photography to reduce errors in final topographies (Harwin and Lucieer, 2012; Valkaniotis et al.,

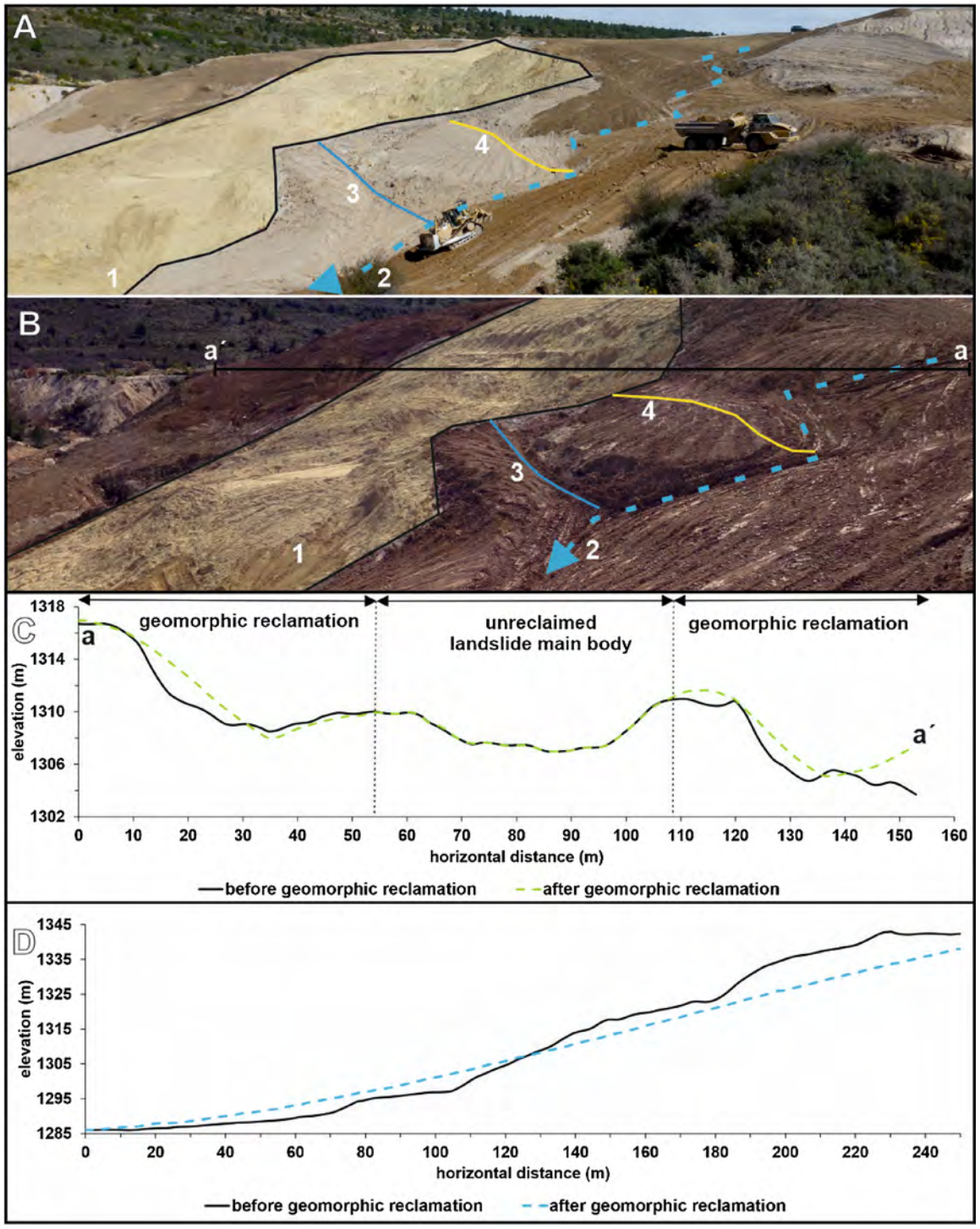


**Fig. 7.** Details of the geomorphic stabilization solution. (A) an articulated truck and a bulldozer finishing the construction by spreading topsoil over one of the regraded valleys; (B) constructed landforms; (C) a-a´ topographic profiles before and after the geomorphic stabilization; (D) longitudinal profile of the constructed left channel (see Fig. 6) before and after the geomorphic stabilization; (1) unreclaimed landslide main body; (2) main zig-zag channel; (3) predominantly concave swale; (4) convex-concave subridge.

2018). In this case, oblique images reduced errors by almost a half.

Although in some instances TLS can be more precise than SfM-UAV (Haas et al., 2016), it often has a lower point density and in complex areas such as landslides can create empty zones (Figs. 9B, C) that can underestimate erosion from DoDs (Haas et al., 2016). The task to obtain a TLS point density identical to SfM-UAV requires a very prolonged field time. Surveying complex slope mining areas can take four hours with a drone as compared to two days by TLS (Haas et al., 2016), as found in the present study. Conversely, TLS survey with the MS60 requires no post-processing time, whereas the SfM-UAV procedure takes several hours to process field data. However, the SfM-UAV processing is almost entirely automated with few hours of supervision to verify control-check points. In addition to the advantages of accuracy increased resolution and reduced field work time, SfM-UAV is also cheaper. The main limiting factor to use the SfM-UAV technique in the Nuria landslide, or in other reclaimed areas, is vegetation growth


**Fig. 8.** Oblique aerial views of the geomorphic stabilization undertaken in the Nuria landslide: at the end of the construction, in May 2015 (A), in November 2017 (B), and in February 2019 (C). The yellow dotted line represents a new geomorphic reclamation, adjacent to the stabilized landslide, completed in September 2017. Photos by DGDRONE. (For interpretation of the references to colour in this figure legend, the reader is referred to the web version of this article).

(Harwin and Lucieer, 2012). Although high point cloud densities (in the range 260–7,985 pts $m^{-2}$) have been obtained with the SfM-UAV, they could have been improved had the drone flight been kept at a constant height above the ground. This can be done by employing different flights at the same altitude relative to the ground with different take-off point locations in several parts of the slope.

## 5. Conclusions

The earth movement at the Nuria mine transformed and degraded almost 50% of a natural catchment, triggering severe environmental effects, such as the occurrence of erosion and landslides. The rotational landslide at the Nuria mine was not the only high risk threatening to the Alto Tajo National Park, but it was one of the principal ones at the end of 2014. For measures of landslide stabilization, a new approach was applied based on geomorphic reclamation. This method had previously been successfully used in mining reclamation projects; however, this is its first use for landslide stabilization, where the environment of a Natural Park claimed for non-structural and ecologic solutions, re-establishing 'naturally' functional and visually appealing landforms.

TLS monitoring and DoDs comparisons allowed demonstrating both the large volume of land transformation by the Nuria mine and the high velocities of the mass movement. They have also demonstrated that geomorphic reclamation was successful in stabilizing the Nuria landslide, by building two 'natural' valleys with fluvial channels, to simultaneously drain surface and ground water, remove the mass of the upper parts of the landslide and strengthen the base of the landslide.

Although a TLS is a reliable instrument to obtain dense point clouds and HRTs in mining areas, the use of SfM-UAV offers better accuracy and higher resolution, is less expensive and faster, providing that vegetation cover is minimal. This method can be used to allow the required monitoring of the long-term evolution of the Nuria landslide. We

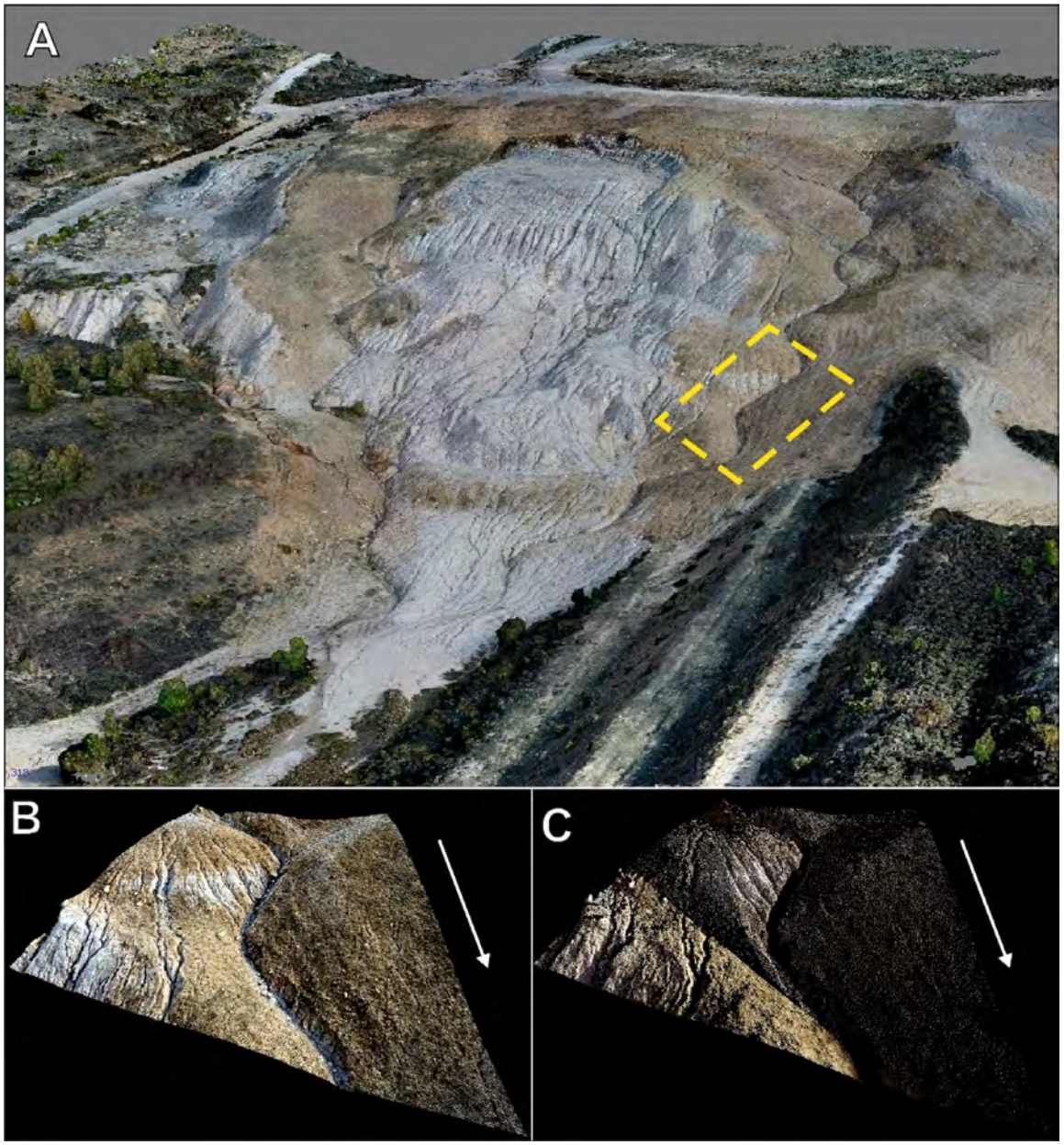


**Fig. 9.** 3D point clouds views surveyed in 2017. (A) General SfM-UAV-based topographic view (oblique and planar photos and "high quality" dense cloud setting); (B) detail of the SfM-UAV topography; (C) detail of the TLS topography. The yellow dashed line shows the location of the detailed B–C area. White arrows denote the direction of water flow. (For interpretation of the references to colour in this figure legend, the reader is referred to the web version of this article).

**Table 3**
Point cloud density, time and accuracy depending on different Agisoft configurations and photo sources compared with TLS scans.

| source | Agisoft dense cloud quality setting | point cloud density[1] | time to produce a final point cloud | | RMSE check points | |
|---|---|---|---|---|---|---|
| | | | field[2] | computer[3] | x, y | z |
| | | pts $m^{-2}$ | h | | m | |
| TLS | | 122.69 | 16 | 0 | 0.068 | 0.038 |
| SfM-UAV with planar and oblique photos | high | 1061.84 | 3 | 58.5 | 0.009 | 0.009 |
| | moderate | 260.32 | | 29 | 0.013 | 0.014 |
| SfM-UAV with planar photos | ultra-high | 7985.19 | 2.8 | 48 | 0.024 | 0.016 |
| | high | 1953.24 | | 12 | 0.024 | 0.019 |
| | moderate | 481.04 | | 3.5 | 0.024 | 0.019 |

[1] Raw point cloud without 'cleaning'.
[2] TLS: inserting control/check marks in the field (2.5 h) and surveying from different locations; SfM-UAV: also requires control/check marks (2.5 h) and drone flying time.
[3] Alignment (highest option) and dense cloud steps.

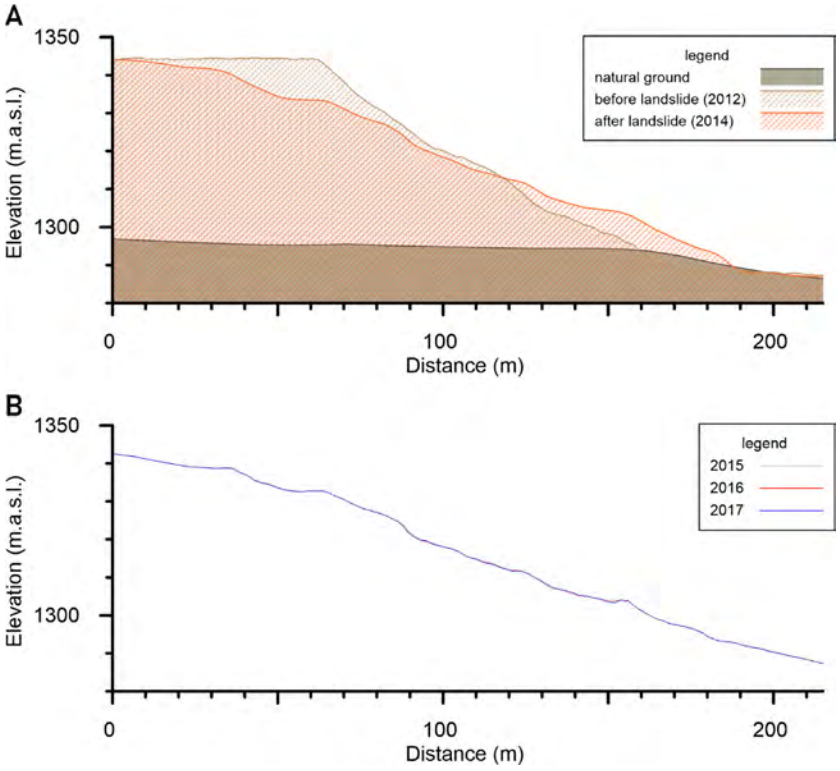


**Fig. 10.** Temporal evolution of the Nuria waste dump main body profile. (A) pre-geomorphic stabilization; (B) post-geomorphic stabilization.

conclude that the described approach of geomorphic stabilization may be ineffective for deep slides. In the case of the Nuria mine this approach has definitely been very effective.

## Acknowledgements

This study was funded by: (i) Research ProjectCGL2010-21754-C02-01 (Spanish Ministry of Science and Technology, and Ministry of Economy); (ii) the Research contract 213/2016 between CAOBAR and UCM; (iii) the Ecological Restoration Network REMEDINAL-3 of the Madrid Community (S2013/MAE-2719); (iv) the postdoctoral grant *Torres Quevedo* (cofounded by the Spanish Ministry of Science, Innovation and Universities and *Diseño y Desarrollo Minero SL* company) to Ignacio Zapico. We thank, E. Taulero, S. Nyssen, M. Tejedor, C. Martín, M. Vara, Á. Vela, R. Ibáñez, R. Ruiz, J.A. Lozano, Á. Moya, J. González, Q. Rubio, J. de la Villa, N. Bugosh, V. Lopez and the staff rangers of the Alto Tajo Natural Park for their support. We especially thank David Gutiérrez (DGDRONE), our drone pilot and aerial filmmaker, and Melanie Ball for English editing of the manuscript. Two anonymous reviewers and the Journal's editor made manifold constructive suggestions.

## References

Agisoft LLC, 2016. Agisoft PhotoScan 1.2.4. Professional Edition.

Agüera-Vega, F., Carvajal-Ramírez, F., Martínez-Corricondo, P., 2017. Assessment of photogrammetric mapping accuracy based on variation ground control points number using unmanned aerial vehicle. Measurement 98, 221–227. https://doi.org/10.1016/j.measurement.2016.12.002.

ASPRS, 2014. ASPRS Positional accuracy standards for digital geospatial data. Photogramm. Eng. Rem. S. 81, A1–A26. https://doi.org/10.14358/PERS.81.3.A1-A26.

Baldo, M., Bicocchi, C., Chiocchini, U., Giordan, D., Lollino, G., 2009. LIDAR monitoring of mass wasting processes: The Radicofani landslide, Province of Siena, Central Italy. Geomorphology 3-4, 193–201. https://doi.org/10.1016/j.geomorph.2008.09.015.

Bugosh, N., 2000. Fluvial Geomorphic Principles Applied to Mined Land Reclamation. OSM Alternatives to Gradient Terraces Workshop, January 2000. Office of Surface Mining, Farmington, NM, United States.

Bugosh, N., Epp, E., 2019. Evaluating sediment production from native and fluvial geomorphic reclamation watersheds at La Plata Mine. Catena 174, 383–398. https://doi.org/10.1016/j.catena.2018.10.048.

Carlà, T., Farina, P., Intrieri, E., Ketizmen, H., Casagli, N., 2018. Integration of ground-based radar and satellite InSAR data for the analysis of an unexpected slope failure in an open-pit mine. Eng. Geol. 235, 39–52. https://doi.org/10.1016/j.enggeo.2018.01.021.

Carrivick, J.L., Smith, M.W., Duncan, J.Q., 2016. Structure From Motion in the Geosciences. John Wiley & Sons, UK. https://doi.org/10.1002/9781118895818.

Di Maio, C., Fornaro, G., Gioia, D., Reale, D., Schiattarella, M., Vassallo, R., 2018. In situ and satellite long-term monitoring of the Latronico landslide, Italy: displacement evolution, damage to buildings, and effectiveness of remedial works. Eng. Geol. 245, 218–235. https://doi.org/10.1016/j.enggeo.2018.08.017.

GCD, 2015. Geomorphic Change Detection Software, Version 6.1.14. (accesed 01.06.2016). http://gcd.joewheaton.org/.

Giordan, D., Allasia, P., Manconi, A., Baldo, M., Santangelo, M., Cardinali, M., Corazza, A., Albanese, V., Lollino, G., Guzzetti, F., 2013. Morphological and kinematic evolution of a large earthflow: the Montaguto landslide, southern Italy. Geomorphology 187, 61–79. https://doi.org/10.1016/j.geomorph.2012.12.035.

Giordan, D., Manconi, A., Tannant, D.D., Allasia, P., 2015. UAV: Low-cost remote sensing for high-resolution investigation of landslides. In: 2015 IEEE International Geoscience and Remote Sensing Symposium (IGARSS). IEEE, Milan. pp. 5344–5347. https://doi.org/10.1109/IGARSS.2015.7327042.

Haas, F., Hilger, L., Neugirg, F., Umstädter, K., Breitung, C., Fischer, P., Hilger, P., Heckmann, T., Dusik, J., Kaiser, A., Schmidt, J., Della Seta, M., Rosenkranz, R., Becht, M., 2016. Quantification and analysis of geomorphic processes on a recultivated iron ore mine on the Italian island of Elba using long-term ground-based lidar and photogrammetric SfM data by a UAV. Nat. Hazard. Earth Sys. 16 (5), 1269–1288. https://doi.org/10.5194/nhess-16-1269-2016.

Harwin, S., Lucieer, A., 2012. Assessing the accuracy of georeferenced point clouds produced via multi-view stereopsis from Unmanned Aerial Vehicle (UAV) imagery. Remote Sens. 4 (6), 1573–1599. https://doi.org/10.3390/rs4061573.

Highland, L.M., Bobrowsky, P., 2008. The Landslide Handbook: a Guide to Understanding Landslides. U.S. Geological Survey Circular 1325, Reston, Virginia. http://pubs.usgs.gov/circ/1325/.

IGN, 1995. Mapa Topográfico Nacional De España 1:25.000. Peralejos De Las Truchas Hoja 539-2. Instituto Geográfico Nacional, Madrid. (in Spanish).

Jaboyedoff, M., Oppikofer, T., Abellán, A., Derron, M.H., Loye, A., Metzger, R., Pedrazzini, A., 2012. Use of LIDAR in landslide investigations: a review. Nat. Hazards Dordr. 61, 5–28. https://doi.org/10.1007/s11069-010-9634-2.

James, M.R., Robson, S., 2014. Mitigating systematic error in topographic models derived from UAV and ground-based. Earth Surf. Proc. Land. 39, 1413–1420. https://doi.org/10.1002/esp.3609.

Javernick, L., Brasington, J., Caruso, B., 2014. Modeling the topography of shallow braided rivers using Structure-from-Motion photogrammetry. Geomorphology 213, 166–182. https://doi.org/10.1016/j.geomorph.2014.01.006.

Lucieer, A., de Jong, S.M., Turner, D., 2014. Mapping landslide displacements using

Structure from Motion (SfM) and image correlation of multi-temporal UAV photography. Prog. Phys. Geog. 38 (1), 97–116. https://doi.org/10.1177/0309133313515293.

Martín-Moreno, C., Martín Duque, J.F., Nicolau Ibarra, J.M., Muñoz, A., Zapico, I., 2018. Waste dump erosional landform stability – a critical issue for mountain mining. Earth Surf. Process. Landf. 43, 1431–1450. https://doi.org/10.1002/esp.4327.

Mezaal, M.R., Pradhan, B., 2018. An improved algorithm for identifying shallow and deep-seated landslides in dense tropical forest from airborne laser scanning data. Catena 167, 147–159. https://doi.org/10.1016/j.catena.2018.04.038.

Nex, F., Remondino, F., 2014. UAV for 3D mapping applications: a review. Appl. Geom. 6, 1–15. https://doi.org/10.1007/s12518-013-0120-x.

Ortuño, M., Guinau, M., Calvet, J., Furdada, G., Bordonau, J., Ruiz, A., Camafort, M., 2017. Potential of airborne LiDAR data analysis to detect subtle landforms of slope failure: portainé, Central Pyrenees. Geomorphology 295, 364–382. https://doi.org/10.1016/j.geomorph.2017.07.015.

PNOA, 2009. Plan Nacional De Ortofotografía Aérea, LiDAR De Castilla la–Mancha, Vuelo De 2009. Instituto Geográfico Nacional, Ministerio de Fomento (Accessed 06.12.2016). (in Spanish). http://pnoa.ign.es/.

PNOA, 2012. Plan Nacional De Ortofotografía Aérea, Ortofoto De Castilla la–Mancha, Vuelo De 2012. Instituto Geográfico Nacional, Ministerio de Fomento (Accessed 06.12.2016). (in Spanish). http://pnoa.ign.es/.

Qcoherent software LLC, 2015. LP360 Advanced Level. (Version 2015.1.76.7).

Rosgen, D.L., 1994. A classification of natural rivers. Catena 22, 169–199. https://doi.org/10.1016/0341-8162(94)90001-9.

Şengör, M.Y., Ergun, M.U., Huvaj, N., 2013. Landslide stabilization by piles: a case history. In: Delage, P., Desrues, J., Frank, R., Puech, A., Schlosser, F. (Eds.), Proceedings of the 18th International Conference on Soil Mechanics and Geotechnical Engineering. Paris. pp. 2253–2256.

Tonkin, T.N., Midgley, N.G., 2016. Ground-Control Networks for Image based Surface Reconstruction: an investigation of optimum survey designs using UAV derived imagery and Structure-from-Motion photogrammetry. Remote Sens. 8 (9), 786. https://doi.org/10.3390/rs8090786.

Toy, T.J., Chuse, W.R., 2005. Topographic reconstruction: a geomorphic approach. Ecol. Eng. 24, 29–35. https://doi.org/10.1016/j.ecoleng.2004.12.014.

Valkaniotis, S., Papathanassiou, G., Ganas, A., 2018. Mapping an earthquake-induced landslide based on UAV imagery; case study of the 2015 Okeanos landslide, Lefkada, Greece. Eng. Geol. 245, 141–152. https://doi.org/10.1016/j.enggeo.2018.08.010.

Victoriano, A., Brasington, J., Guinau, M., Furdada, G., Cabré, M., Moysset, M., 2018. Geomorphic impact and assessment of flexible barriers using multi-temporal LiDAR data: the Portainé mountain catchment (Pyrenees). Eng. Geol. 237, 168–180. https://doi.org/10.1016/j.enggeo.2018.02.016.

Xiang, J., Chen, J., Sofia, G., Tian, Y., Tarolli, P., 2018. Open-pit mine geomorphic changes analysis using multi-temporal UAV survey. Environ. Earth Sci. 77, 220. https://doi.org/10.1007/s12665-018-7383-9.

Yu, Y., Shen, M., Sun, H., Shang, Y., 2019. Robust design of siphon drainage method for stabilizing rainfall-induced landslides. Eng. Geol. In press. https://doi.org/10.1016/j.enggeo.2019.01.001.

Zapico, I., Laronne, J.B., Martín-Moreno, C., Martín-Duque, J.F., Ortega, A., Sánchez-Castillo, L., 2017. Baseline to evaluate off-site suspended sediment-related mining effects in the Alto Tajo Natural Park. Spain. Land Degrad. Dev. 28 (1), 232–242. https://doi.org/10.1002/ldr.2605.

Zapico, I., Martín Duque, J.F., Bugosh, N., Laronne, J.B., Ortega, A., Molina, A., Martín-Moreno, C., Nicolau, J.M., Sánchez, L., 2018. Geomorphic Reclamation for re-establishment of landform stability at a watershed scale in mined sites: the Alto Tajo Natural Park. Spain. Ecol. Eng. 111, 100–116. https://doi.org/10.1016/j.ecoleng.2017.11.011.